HIGH-RESOLUTION OU-PRIME RADAR OBSERVATIONS OF A PROLIFIC TORNADO-PRODUCING SUPERCELL ON 10 MAY 2010

D. Bodine[1,2,*], R. D. Palmer[1,2], M. R. Kumjian[1,3], and A. V. Ryzhkov [4]

[1] School of Meteorology, The University of Oklahoma, Norman, OK, U.S.A.
[2] Atmospheric Radar Research Center, The University of Oklahoma, Norman, OK, U.S.A
[3] Cooperative Institute for Mesoscale Meteorological Studies, The University of Oklahoma, Norman, OK, U.S.A
[4] NOAA/OAR National Severe Storms Laboratory, Norman, OK, U.S.A

1. INTRODUCTION

Some of the most deadly tornado outbreaks occur with cyclic supercells (e.g., Fujita, 1975), hence understanding their evolution is pivotal to minimizing the risks associated with cyclic supercells. Observational studies have noted a cyclic redevelopment of low-level mesocyclones and, in some cases, tornadoes (e.g., Darkow and Roos, 1970; Lemon and Doswell, 1979; Burgess et al., 1982; Dowell and Bluestein, 2002a,b; Beck et al., 2006; French et al., 2008). These studies have elucidated the kinematic properties of cyclic mesocyclogenesis, and conceptual models have been developed from these studies (e.g., Burgess et al., 1982; Dowell and Bluestein, 2002a,b). Numerical simulations of cyclic supercells have also been performed, confirming the conceptual models of cyclic mesocyclogenesis and tornadogenesis (Adlerman et al., 1999; Adlerman and Droegemeier, 2002, 2005). In brief, in the beginning stage of a cyclic supercell, discrete vorticity maxima develop along the rear-flank downdraft (RFD) gust front, whereupon they move to the left (with respect to storm motion) and occlude. During the occlusion, a new vorticity maximum forms along the surging RFD gust front, and the cycle repeats.

While these studies of cyclic supercells have significantly advanced our understanding of the dynamics of cyclic supercells, the idealized case of a cyclic supercell is not always observed. Storm interactions, including storm mergers (e.g., Byers and Braham, Jr., 1948), can complicate the dynamics of cyclic supercells and other severe storms. In some cases, tornadogenesis occurs almost simultaneously with the storm merger (e.g., Lee et al., 2006; Wurman et al., 2007); while in other cases, the storm becomes more disorganized and tornadogenesis is inhibited. Wurman et al. (2007) suggest that further studies are needed to understand how the geometry of the storm merger, size and intensity of the merging storm, affect the evolution of the parent storm after the merger. In a study of the 26 storm mergers, Lee et al. (2006) found that 54 percent of tornadoes occurred after a storm merger during the 19 April 1996 tornado outbreak. In addition to storm mergers, storms in close proximity can positively or negatively impact each other, and the nature of these interactions is not fully understood. One example of storm interactions includes an outflow boundary produced by a nearby storm that moved beneath another storm, which is generally favorable for tornadogenesis (e.g., Markowski et al., 1998). A better understanding of the evolution of storm dynamics during storm interactions (particularly storm mergers) is required to determine whether the storm interactions are beneficial or detrimental to storm evolution.

The emergence of polarimetric radar observations of supercells has advanced our understanding of the microphysics of such storms (e.g., Conway and Zrnić, 1993; Hubbert et al., 1998; Loney et al., 2002; Kumjian and Ryzhkov, 2008; Romine et al., 2008). Kumjian and Ryzhkov (2008) found several distinct, commonly observed polarimetric signatures associated with numerous supercell storms. These signatures, while providing information about bulk microphysical properties in the storm, are also related to kinematic features of supercells such as updrafts, downdrafts, the mesocyclone, and even storm-relative helicity in the inflow environment (Kumjian and Ryzhkov, 2009).

However, most of the aforementioned studies are limited by relatively coarse spatial and temporal resolution, and thus do not adequately investigate the evolution of microphysical processes in supercell storms throughout the cyclic occlusion process. To date, only one paper (Kumjian et al., 2010) has investigated the evolution of the polarimetric radar signatures through the occlusion cycle. Using a rapid scanning strategy (about 71 s volumes), they found a repetitive pattern of the signatures seemingly related to cyclic mesocyclogenesis, albeit for one case. In the present study, polarimetric radar data from the University of Oklahoma Polarimetric Radar for Innovations in Meteorology and Engineering (OU-PRIME) are examined to investigate if a similar repetitive pattern in polarimetric signatures is observed in a tornadic cyclic supercell, and what differences are observed (e.g., are they different for the tornadic and nontornadic case?).

This paper also examines how storm interactions affect the genesis, maintenance and dissipation of tornadoes in cyclic supercells. In particular, the 10 May 2010 case is unique because two cyclic supercells undergo storm mergers and

* *Corresponding author address:* David Bodine, University of Oklahoma, School of Meteorology, 120 David L. Boren Blvd., Rm 4630, Norman, OK 73072-7307; e-mail: bodine@ou.edu

remain in close proximity to each other throughout their evolution. Moreover, polarimetric data are examined during storm mergers to determine the impact of the merger on the structure of the parent storm. The evolution of these polarimetric supercell signatures may illuminate changes in storm dynamics and microphysics occurring during the storm merger, and the consequences of the storm mergers and interactions on cyclic mesocyclogenesis and tornadogenesis.

OU-PRIME (Palmer et al., 2009, 2010) collected a rare polarimetric dataset during the 10 May 2010 tornado outbreak in central Oklahoma, capturing high-resolution polarimetric data from several supercells, and nearly a dozen tornadoes in close proximity to OU-PRIME. A brief overview of the 10 May 2010 tornado outbreak is presented in Section 2a, followed by a technical description of OU-PRIME (Palmer et al., 2009, 2010) and the 10 May 2010 dataset in Section 2b. This paper examines OU-PRIME data from two cyclic supercells that produced both violent tornadoes. The northern supercell (Supercell A) produced an EF4 tornado that struck Moore, Oklahoma and southern Oklahoma City, and is discussed in more depth in a companion paper (Bodine et al., 2010). The southern supercell (Supercell B) produced an EF4 tornado that developed just 200 yards from OU-PRIME, and an EF3 tornado that struck Tecumseh and Seminole, Oklahoma. The analysis in Section 3 examines Supercell B's evolution during a full occlusion cycle and investigating storm interactions occurring with Supercell A. The paper concludes with a summary and discussion of results in Section 4.

2. OUTBREAK OVERVIEW AND DATA DESCRIPTION

2.1. 10 May 2010 Overview

The 10 May 2010 tornado outbreak produced 35 tornadoes in Oklahoma, including seven strong and two violent tornadoes (Figure 1). Two deaths were reported and extensive property damage was sustained. Fortunately, the outbreak was very well forecasted, as the synoptic environment clearly signaled a major severe weather outbreak, and the Storm Prediction Center issued a high risk of severe weather in central and eastern Oklahoma. The reader is referred to the discussion on the environmental conditions leading to the outbreak by Palmer et al. (2010), although it is discussed briefly here.

A special 2100 UTC Norman, Oklahoma sounding (Figure 2) on 10 May 2010 was a classic "loaded gun" sounding (Fawbush and Miller, 1952), with very high CAPE (about 3000 J kg^{-1}) and a substantial hydrolapse above the convective boundary layer. The most striking component of the radiosonde measurements is the extraordinarily high vertical wind shear, particularly in the lowest 1 km AGL. The storm-relative helicity (SRH) in the 0-1 km layer was over 300 J kg^{-1}, which is above the 90th percentile of SRH values in significant tornadoes events, based on Rasmussen (2003).

In addition to very high wind shear and instability, high surface and boundary layer moisture were observed during the 10 May 2010 outbreak. East of the dryline at 2200 UTC, surface dewpoint depressions were between 5 and 7°C and surface relative humidities were between 65 and 70 percent. Moist surface conditions are more favorable for signficant tornadoes because of lower lifted condensation levels (LCLs; Rasmussen and Blanchard, 1998). A nearly saturated layer is also observed in the 2100 UTC sounding between 900 and 830 hPa, and the mean boundary layer humidity is over 80 percent. Markowski et al. (2002) found that high boundary layer humidities produce more buoyant rear-flank downdrafts (RFDs) and increase the likelihood of tornadoes.

2.2. Data

A detailed technical description of OU-PRIME is presented by Palmer et al. (2010), although a brief description is provided here for completeness. OU-PRIME possesses a 0.45° beamwidth, and range resolution up to 25 m with oversampling, making it one of the highest resolution C-band polarimetric radars in the world. During the 10 May 2010 outbreak, the radar employed a longer pulse width to increase sensitivity, so the range resolution was 125 m. In addition to high spatial resolution, OU-PRIME has a peak transmit power of 1 MW, providing excellent sensitivity. During the 10 May 2010 outbreak, sector mode scanning by OU-PRIME improved update times to 2–3 min without compromising data quality (e.g., without decreasing the number of pulses). The radar operated with an unambiguous velocity of 16 m s^{-1}, hence significant velocity folding occurred within high shear regions such as within the tornado. To improve the unambiguous velocity, future plans include implementing methods for increasing the maximum unambiguous velocity, such as a staggered PRT (Sirmans et al., 1976).

After data collection, several steps were taken to generate high quality radar data. First, clutter filtering was applied to the time series data, and then moment data were produced using the multi-lag estimator (Zhang et al., 2004; Lei et al., 2009). The National Center for Atmospheric Research (NCAR) Solo-II software package was employed to remove noise and second-trip echoes (Oye et al., 1995). A signal-to-noise threshold of -5 dB was applied to all fields to remove suspect data in noisy regions. After data post-processing, OU-PRIME data are imported into the Warning Decision Support System - Integrated Information (WDSSII; Lakshmanan et al., 2007) display. PPI and RHI plots were generated using the WDSSII display.

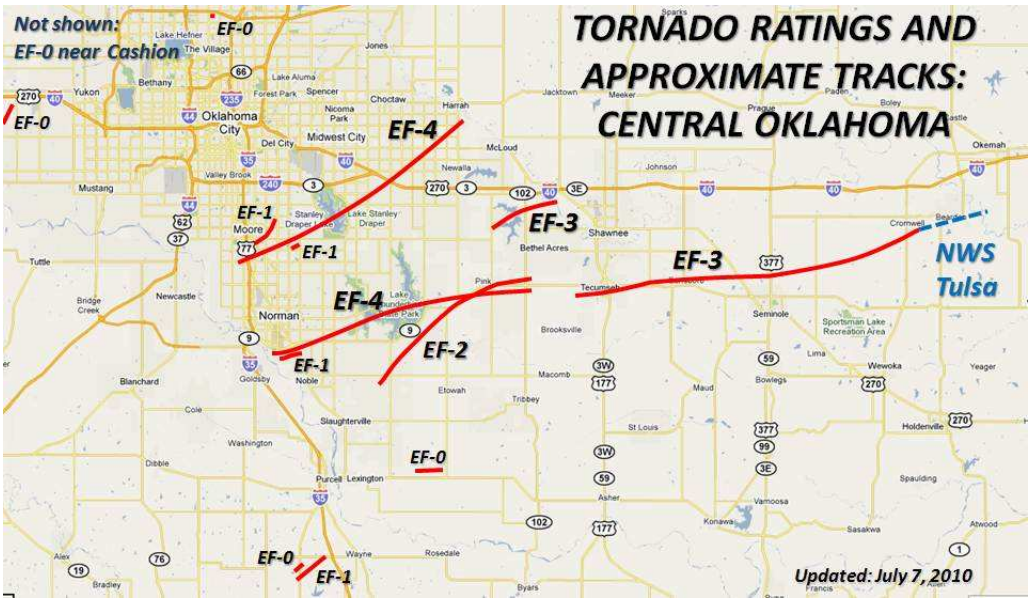

Figure 1: Tornado damage paths in central Oklahoma during the 10 May 2010 tornado outbreak. (courtesy of the Norman National Weather Service Weather Forecast Office; NWS WFO)

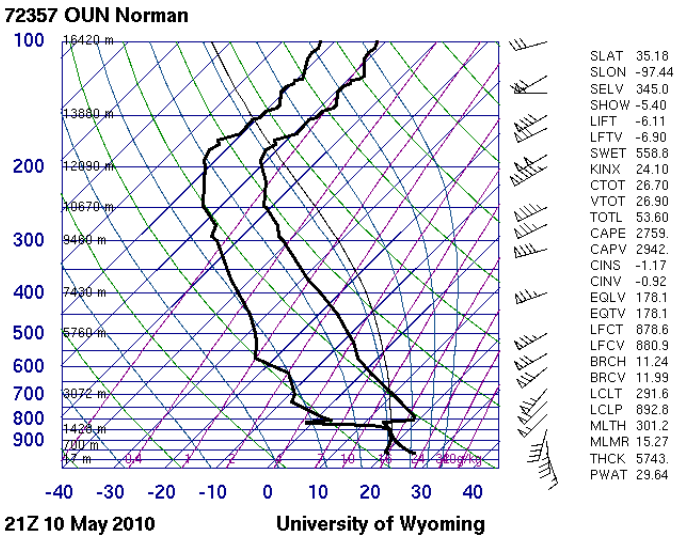

Figure 2: Sounding from Norman, OK (OUN) at 2100 UTC 10 May 2010 (courtesy of the University of Wyoming sounding archive).

To supplement the OU-PRIME data, WSR-88D data and Oklahoma Mesonet (hereafter Mesonet; Brock et al., 1995; McPherson et al., 2007) data were obtained for select sites between 2200 – 0000 UTC. Oklahoma City, Oklahoma (KTLX) and Vance Air Force Base, Oklahoma (KVNX) WSR-88D reflectivity and velocity data are investigated. The WSR-88D data provide coverage at higher tilts, additional data outside of OU-PRIME's sector, and data after 2300 UTC. Another advantage of KTLX data is the reduction in attenuation at S-band compared to C-band, so WSR-88D are examined to assess storm intensity in suspected regions of attenuation. Differential attenuation is a disadvantage of a C-band polarimetric radar (Tabary et al., 2009), however OU-PRIME is a research radar and attenuation correction schemes using polarimetric data are an opportunity for research (Bringi et al., 1990; Vulpiani et al., 2008).

3. ANALYSIS

In this section, the occlusion of the Supercell B is examined, focusing on the evolution of polarimetric signatures. After the occlusion of Supercell B, Supercell A produces a tornado in the FFD of Supercell B. The effect of Supercell A's mesocyclone ingesting air parcels from Supercell B's FFD is investigated. To conclude the analysis, the polarimetric signatures during mesocyclogenesis and cyclic tornadogenesis are discussed as Supercell B develops a new mesocyclone and subsequently an EF3 tornado. The impact of several storm mergers and other storm interactions

during tornadogenesis and tornado intensification are examined.

3.1. Occlusion of the Norman EF4 tornado

Prior to the occlusion of Supercell B, the Z_{DR} arc exhibits a similar evolution to the cyclic supercell presented in Kumjian et al. (2010). At 2242 UTC, the Z_{DR} arc extends along the reflectivity gradient on southern edge of the FFD, with distinct regions of very high Z_{DR} values (Figure 3) protruding from the southern edge of the FFD ($>$ 7 dB). Kumjian et al. (2010) attributed these very high Z_{DR} values to melting hail or graupel, and similar findings here are discussed shortly. The Z_{DR} arc also extends back into the very thin hook echo, where high Z_{DR} values ($>$ 5 dB) are confined to a narrow region as small as 375 m in width.

By 2247 UTC, the areal extent of the Z_{DR} arc reaches a maximum, with a very large region of very high Z_{DR} values observed on the eastern half of the FFD. Closer to the updraft, the band of high Z_{DR} values along the FFD contracts in width compared to 2244 UTC. To the south of the Z_{DR} arc near the updraft, an elongated region of low Z_{DR} ($<$ 2 dB) and high ρ_{hv} values ($>$ 0.97) exists, indicating small drops. Intriguingly, this region of small drops exists only during the 2247 UTC, as Z_{DR} values increase in this region by 2249 UTC. These small drops could have originated in the storm to the south, and been transported by strong, southerly surface inflow. On the eastern flank of the FFD, a large region of high Z_{DR} values is still observed at 2249 UTC, however the area of very high Z_{DR} values is significantly reduced. The Z_{DR} arc near the updraft no longer forms a continuous band of high Z_{DR} values, and has embedded low Z_{DR} values ($<$ 2 dB).

Vertical cross sections of Z_{DR} and ρ_{hv} are quite revealing as to the origins of these large drops, and show two distinct regions (Figure 5). In the lowest 1.2 km AGL, very high Z_{DR} values are present and moderate ρ_{hv} , indicating very large drops. Above 1.2 km AGL, Z_{DR} values are near zero and ρ_{hv} values range from 0.98 to 1.00, suggesting the presence of graupel throughout this region. Hence, melting graupel from above 1.2 km AGL is producing the large drop region in the FFD, consistent with Kumjian et al. (2010).

3.2. The Pink EF3 tornado

This section discusses the genesis, evolution, and dissipation of the Pink EF3 tornado, and investigates the role of heavy precipitation from Supercell A and B's FFDs during the tornado's evolution. During the occlusion of the Norman EF4 tornado, a new low-level mesocyclone forms on the north side of the forward-flank downdraft (FFD) of Supercell B. At 2242 UTC, the low-level mesocyclone

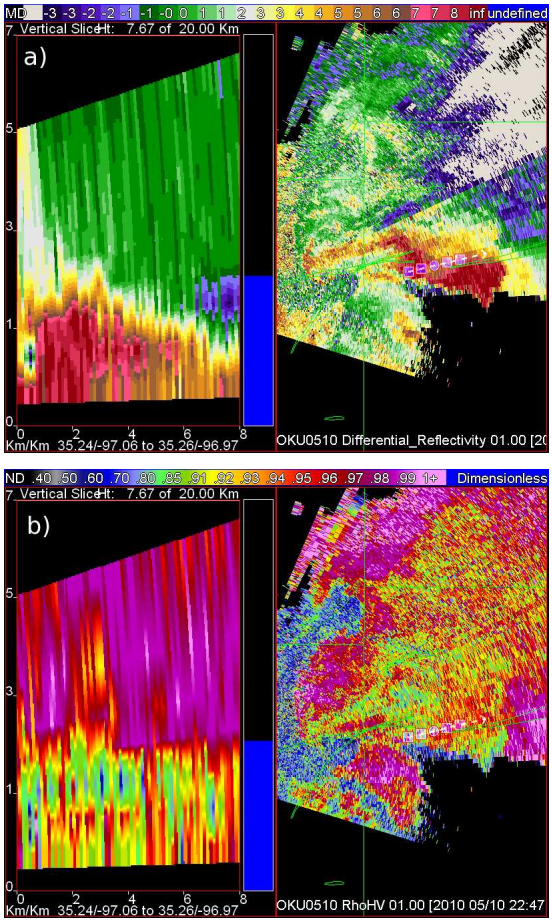

Figure 5: RHI of a) differential reflectivity Z_{DR}, and b) cross correlation coefficient ρ_{hv} at 2247 UTC through Supercell B's FFD. Above 2 km AGL, near zero or slightly negative Z_{DR} values are observed collocated with very high ρ_{hv}, indicating graupel. Below 2 km AGL, Z_{DR} values are much higher and ρ_{hv} values are between 0.91 and 0.96, indicating predominately large drops.

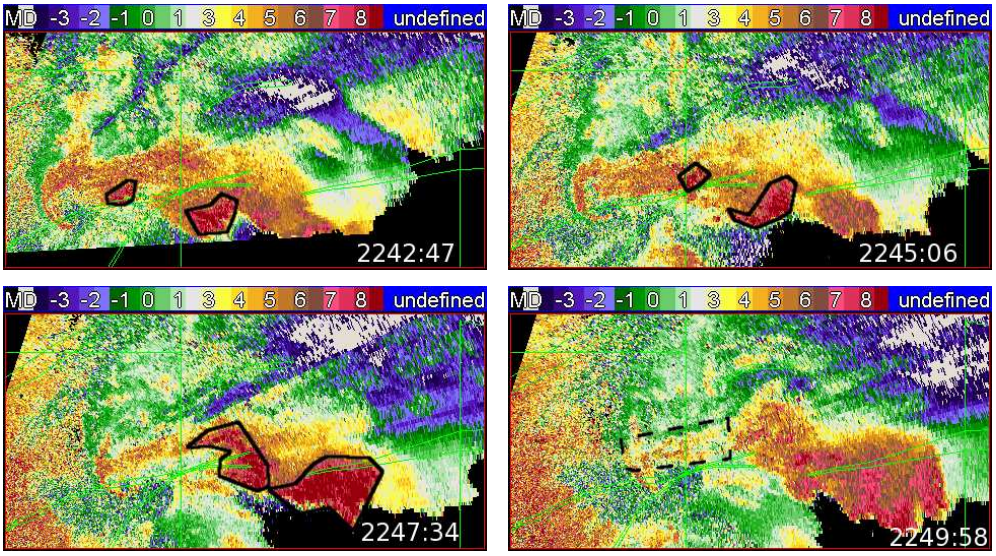

Figure 3: 1°-tilt differential reflectivity Z_{DR} at 2242, 2245, 2247 and 2249 UTC on 10 May 2010. In the 2242 – 2247 UTC panels, regions of very high Z_{DR} are seen along the southern periphery of the FFD, enclosed by the black lines. At 2249 UTC, the Z_{DR} arc dissipates on the southern flank closest to the updraft in the region enclosed by the dashed black line.

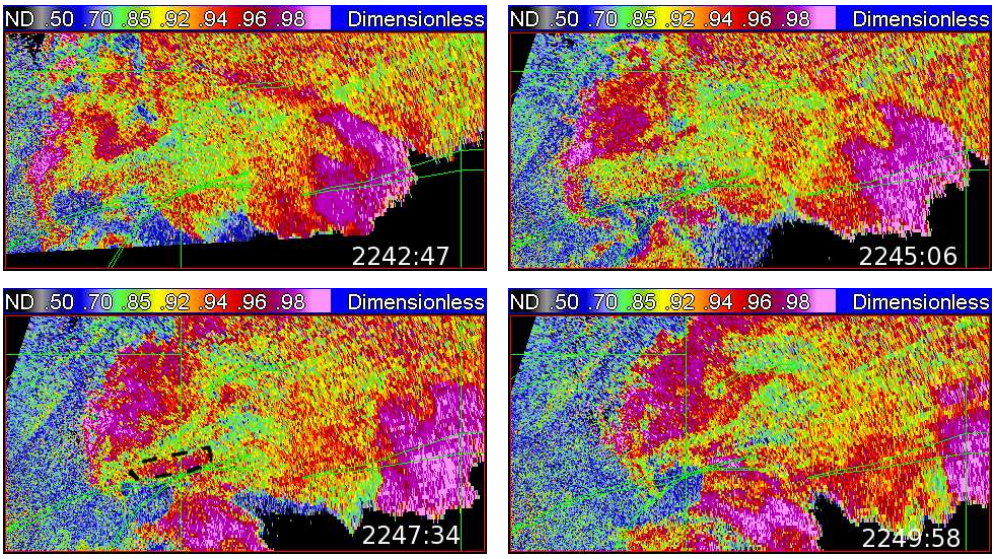

Figure 4: 1°-tilt cross correlation coefficient ρ_{hv} at 2242, 2245, 2247 and 2249 UTC on 10 May 2010. A small region (demarcated by the black dashed line) of very high ρ_{hv} and low Z_{DR} values is observed along the FFD near the updraft, indicating small drops.

exhibits a convergent signature in velocity, indicating imminent intensification of the low-level mesocyclone (e.g., Burgess and Magsig, 1993). The mesocyclone exhibits good vertical continuity and is observed through the 9° tilt (about 5 km AGL). The correlation coefficient and differential reflectivity fields reveal a ρ_{hv} minimum and a local maximum in Z_{DR} collocated with the mesocyclone at 9° tilt. Although significant differential attenuation has occurred, the relatively high Z_{DR} values suggest the presence of large drops or wet hail in the updraft.

As discussed previously, the updraft and tornado develop in the FFD of the northern supercell and are enshrouded by heavy precipitation (Z $>$ 45 dBZ) during tornadogenesis. Precipitation ingested by an updraft can weaken the updraft and lead to the occlusion of the mesocyclone (Lemon and Doswell, 1979), and generally colder air in precipitation reduces the likelihood of tornadogenesis by decreasing the buoyancy of parcels ingested by the developing tornado (Markowski et al., 2002). Hence, how is an EF3 tornado produced within a region of heavy precipitation?

To investigate the impact of precipitation in the FFD on buoyancy, Oklahoma Mesonet data from the Shawnee, Oklahoma Mesonet station (SHAW) are examined. The SHAW station is located in the FFD during most of the 2240 – 2300 UTC timeframe. Relative to the FFD's position, the SHAW station is positioned in the eastern part of the FFD at 2245 UTC and in the western end of the FFD at 2300 UTC. Prior to the arrival of the FFD at about 2245 UTC, the equivalent potential temperature, θ_e, values fluctuate between 73.5 and 74°C. The arrival of the FFD is characterized by a change in wind direction from southeast to northeast, an increase in precipitation, and a decrease in θ_e. Between 2245 and 2305 UTC, θ_e decreases from 73.2 to 72.4°C.

θ_e deficits (hereafter, θ_e') are computed to determine the difference in buoyancy between the environment and the RFD or FFD (e.g., Markowski et al., 2002; Shabbott and Markowski, 2006). In the present case, θ_e' is computed between the environment and the FFD using the mean θ_e during the 30 min prior to the arrival of the FFD. Unfortunately, the absence of observations in the RFD precludes a similar analysis examining the thermodynamic characteristics of the RFD using surface observations. The largest θ_e' is -1.5°C, indicating that the buoyancy in the FFD is very similar to the environment. Thus, even though heavy precipitation (above 50 dBZ at 0.5° tilt from KTLX; not shown) surrounds the low-level mesocyclone and tornado, the parcels ingested into the low-level mesocyclone and tornado are likely still buoyant. However, the effects of water loading on the updraft may weaken the updraft and tornado.

The Pink tornado produced EF3 damage and a 6.5-mile damage path prior to dissipation. At 2250 UTC, KTLX velocity data reveal a large tornado with the RFD gust front remaining relatively close to the tornado (not shown). The highest radial velocities of 50.5 m s^{-1} are observed in the tornado by KTLX occur at 2254 UTC (Table 1), which is in the range of winds for an EF2 tornado. Given the relatively poor temporal sampling relative to the tornado's evolution and the coarse spatial resolution, the winds within the tornado are likely faster.

The tornado weakens between 2254 and 2259 UTC, and the RFD gust front advances eastward relative to the tornado. By 2304 UTC, the tornado is no longer observed in the radial velocity data. The southern part of the RFD gust front associated with Supercell B moves 9 km between the 2259 and 2304 UTC volume scans, or 30 m s^{-1}. The radial convergence along the northern part of the RFD gust front is also much weaker compared to the previous three volume scans, indicating a weakened updraft. While the surging RFD gust front is detrimental to the Pink EF3 tornado, Supercell B undergoes a new cycle during two storm mergers, which is discussed in the next section.

3.3. Reorganization of Supercell B and the Tecumseh EF3 tornado

Supercell B undergoes rapid mesocyclogenesis between 2252 – 2259 UTC, and forms a tornado at about 2259 UTC. Supercell B also merges with several precipitation cores that originate from a storm to the south (Storm C), and eventually merges with Storm C. This section discusses the evolution of Supercell B during mesocyclogensis and the impact of the storm merger on mesocyclogenesis and tornadogenesis. By examining polarimetric signatures, the dynamic evolution of the cyclic supercell can be examined.

1) Z_{DR} ring regeneration

During mesocyclogenesis, the updraft exhibits a persistent Z_{DR} column and eventually develops a prominent Z_{DR} ring (Kumjian and Ryzhkov, 2008; Kumjian et al., 2010). At 2249 UTC, the Z_{DR} column is observed above the environmental freezing level (about 3750 m based on the 2100 UTC OUN sounding), however a Z_{DR} ring is not observed at the 9.0° tilt (Figure 7). The relatively disorganized appearance of Z_{DR} in the updraft and the absence of a Z_{DR} ring may be attributed either to the absence of a strong mesocyclone or insufficient time for vertical vorticity to act on hydrometeors in the mesocyclone. By 2251 UTC, the areal extent of high Z_{DR} values increased, indicating both an increase in drop size and larger drops covering a larger region in the updraft. As discussed in Kumjian et al. (2010), the increase in drop size could be attributed to an increase in updraft strength or large drops falling into the updraft from above.

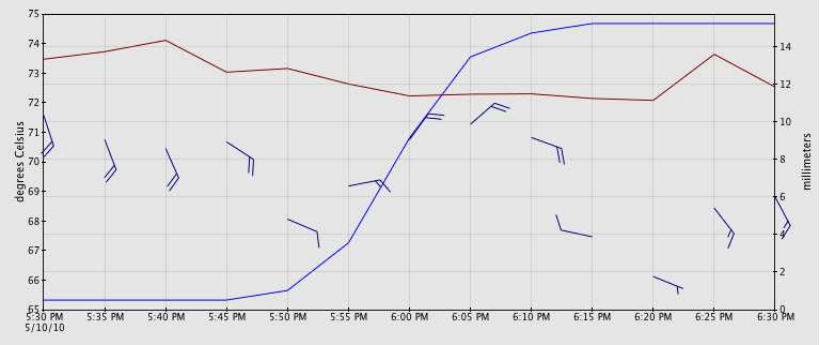

Figure 6: Equivalent potential temperature in °C (θ_e, brown line), rainfall total in mm (blue line), and wind barb from the SHAW Mesonet site between 0530 and 0630 PM LT. The half and full wind barbs are 2.5 and 5 m s^{-1}, respectively. As the FFD passes over the SHAW site between 0545 and 0610 PM LT, θ_e decreased from 73.2 to 72.4°C.

Table 1: Maximum radial velocity, velocity difference, and displacement between the tornado and the RFD gust front (Tornado-RFDGF Displacement) at the 0.5° tilt from KTLX. The position of the tornado at 2304 UTC is based on the low-level mesocyclone since the tornado has dissipated.

Time (UTC)	Max. v$_r$ (m s^{-1})	Velocity Difference (m s^{-1})	Tornado-RFDGF Displacement (km)
2250:55	45.5	63.5	5
2254:09	50.5	84.5	6
2259:44	36.0	40.0	8

A partial Z_{DR} ring develops on the western, southern and southeastern part of the mesocyclone by 2254 UTC. The Z_{DR} ring may not extend into the northern or eastern parts of the mesocyclone, or may not be observed owing to differential attenuation. Strong differential attenuation extends radially outward from the the northern part of the mesocyclone, which could explain the absence of the Z_{DR} ring in the northeast part of the mesocyclone. However, a full ρ_{hv} ring (Kumjian and Ryzhkov, 2008; Kumjian et al., 2010) is observed around the mesocyclone (not shown). Furthermore, the centers of the Z_{DR} and ρ_{hv} rings are roughly collocated with the maximum cyclonic azimuthal shear, consistent with the findings of Payne et al. (2010).

An intriguing evolution occurs with the occluding mesocyclone between 2256 and 2301 UTC. During the 2256 UTC volume scan, the Z_{DR} ring associated with the new mesocyclone is obscured by precipitation ingested from a merging storm, which is discussed in an upcoming section. However, the occluded mesocyclone intensifies and large drops (indicated by high Z_{DR} values) from the Z_{DR} column are advected cyclonically around the occluded mesocyclone. By 2258 UTC, the high Z_{DR} values have wrapped around the western side of the occluded mesocyclone, presumably due to increased horizontal advection associated with an increase in vorticity in the occluded mesocyclone. The Z_{DR} ring associated with the new mesocyclone is better defined, and a full ρ_{hv} ring is also observed. Interestingly, the occluded mesocyclone moves closer to the new mesocyclone during this period whereas in the traditional model of cyclic supercells, the occluded mesocyclone moves away from the new mesocyclone. However, the decrease in diameter and increase in vorticity of the occluded mesocyclone are consistent with French et al. (2008), who also observed similar trends in diameter and vorticity in a subset of occluding mesocyclones.

2) Z_{DR} arc

The Z_{DR} arc reforms very quickly after dissipating between 2247 and 2252 UTC (Figure 8). Between 2247 and 2252 UTC, Z_{DR} values in the eastern half of the FFD decrease. Furthermore, the band of high Z_{DR} values associated with the Z_{DR} arc in the updraft region contract into an even smaller region, although a continuous band of relatively high Z_{DR} values (between 2 – 5 dB) still extends through the hook echo. By 2254 UTC, the high Z_{DR} values in the hook echo diminish to 1 – 3 dB. The decrease in drop size may result from differential sedimentation (Kumjian and Ryzhkov, 2009). After the occlusion, the difference in terminal velocities of different drop sizes causes the large drops to fall faster and reach the surface first while the smaller drops take longer to fall and arrive later.

While the old Z_{DR} arc has fully dissipated, a new Z_{DR} arc is developing along the southern FFD at 2254 UTC. The new Z_{DR} arc forms south of high Z_{DR} values remaining from the old Z_{DR} arc. The Z_{DR} arc extends further back toward the low-level mesocyclone by 2257 UTC, and Z_{DR} values along the eastern FFD decrease significantly, accompanied by an increase in ρ_{hv} and a decrease in Z (not shown), indicating a decrease in drop size. The reduced drop size may also result from differential sedimentation since as the production of large drops ceases, the large drops fall out first followed by small drops. Since the storm's updraft was likely weakened during the storm merger, the small drops could also result from a brief disruption in hail and graupel growth owing to a weakened updraft. At 2259 UTC, the Z_{DR} arc is very well defined, extending back around the western side of the newly formed tornado. The spatial variability of Z_{DR} in the Z_{DR} arc is much smaller compared to the very high spatial variability observed during the occlusion.

3) Impact of first storm merger on mesocyclogensis and tornadogenesis

Supercell B merges with three separate precipitation cores between 2252 and 2259 UTC. The merger of this shallow, incipient convection (hereafter, called Storm C1, C2, and C3) with Supercell B further complicated the evolution of Supercell B during these mergers. Intriguingly, the size, intensity, and bulk microphysics of each precipitation core varies significantly. Although the first precipitation core (Storm C1) moves to the left of the mean wind, suggestive of storm splitting, the structure of a left-moving storm is not observed. Furthermore, radial velocity does not reveal anticyclonic rotation typically observed in a left-moving supercell. The structure of the second precipitation core (Storm C2) appears closer to a left-split, however anticyclonic rotation is not observed. The remnants of Storm C (Storm C3) finally merge with Supercell B during the 2257 and 2259 UTC volume scans. For reference, tornadogenesis occurs at 2256 UTC according to the damage survey provided by the Norman NWS WFO, although a clear velocity signature does not appear until 2259 UTC.

The first precipitation core (Storm C1), observed during the 2252 UTC volume scan, is characterized by a gradient in drop sizes from north to south. On the northern end, Storm C1 has very high ρ_{hv} ($>$ 0.99), low Z_{DR} ($<$ 2.5 dB), and low to moderate Z (25 – 35 dBZ), suggesting predominately small drop sizes. Larger drop sizes were found on the southern end of Storm C1, with high ρ_{hv} (about 0.97), moderate Z_{DR} values (2 – 4 dB), and slightly higher Z (30 – 40 dBZ). A small reflectivity tail extends from Storm C1 at 2253:47 UTC, and the orientation of the tail rotates counter-clockwise with height during the 2252 UTC volume scan, indicative of cyclonic rotation in the updraft. The gradient of drop sizes may result from the faster transport of the smaller

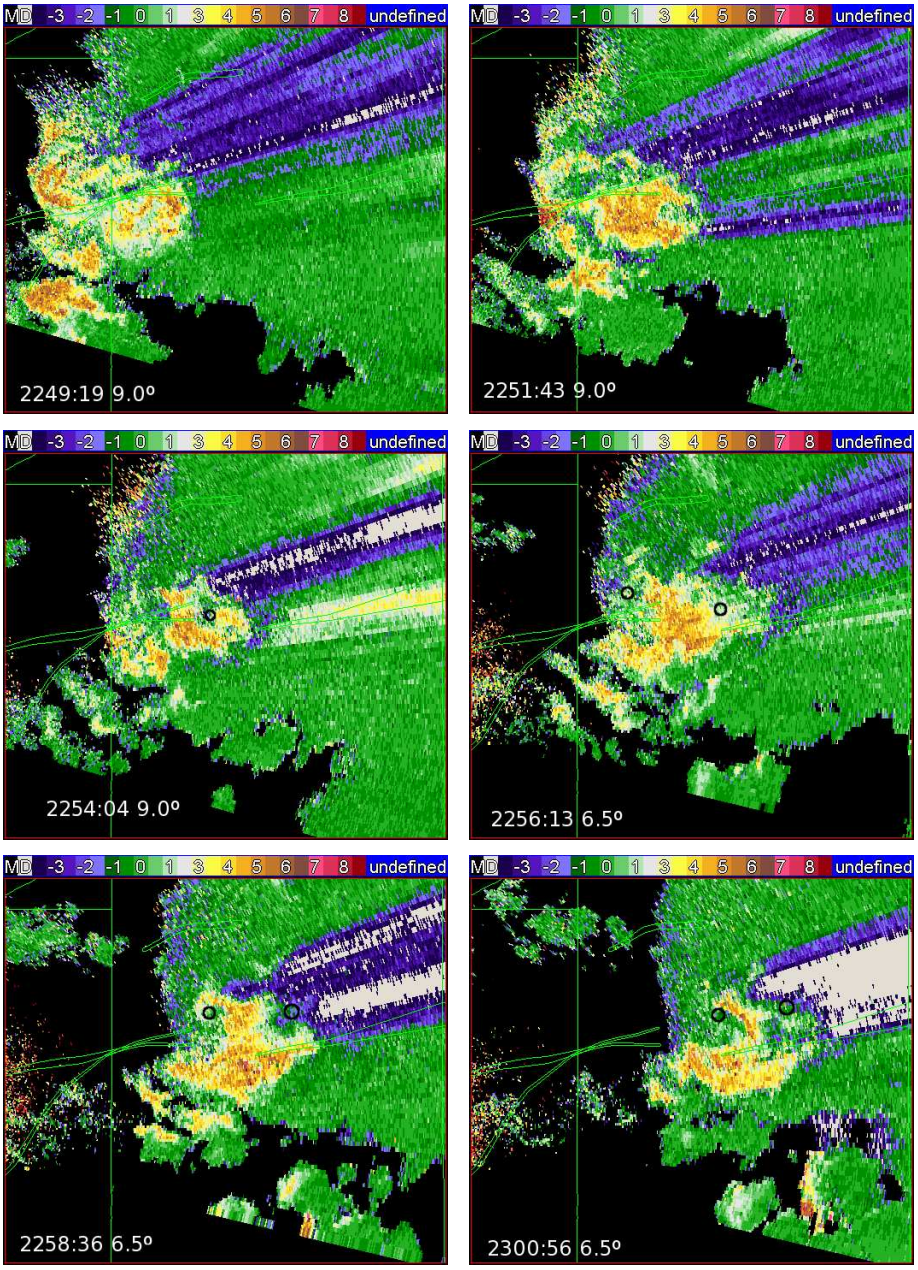

Figure 7: Evolution of the differential reflectivity Z_{DR} ring between 2249 – 2301 UTC 10 May 2010, shown at 9.0°for 2249 – 2254 UTC and 6.5°at 2256 – 2301 UTC. The Z_{DR} ring is located at between 5 – 6 km in the tilts shown. The black circle on select panels indicates the center of the mesocyclone or occluded mesocyclone based on radial velocity data.

drops compared to larger drops into the updraft as Storm C1 merges with Supercell B.

The second precipitation core (Storm C2), observed during the 2254 UTC volume scan, exhibits a more uniform spatial distribution of drop sizes. Precipitation in Storm C2 has moderate Z_{DR} (2 – 5 dB), moderate ρ_{hv} values (0.90 – 0.97), and higher reflectivity (35 – 45 dBZ), indicating moderate drop sizes and moderate drop concentration. Storm C2 moves into the updraft region of Supercell B by 2255:50 UTC. The ingestion of these large drops produces a relatively disorganized appearance in Z_{DR} at upper levels, as a clear Z_{DR} ring is not observed (Figure 7; 2256 UTC at 6.5°). However, by 2259 UTC, a partial Z_{DR} ring and a full ρ_{hv} ring are observed at 6.5° tilt, suggesting that the storm quickly reorganized after the storm merger.

In contrast, at low-levels, the Z_{DR} arc forms and extends back into the low-level mesocyclone and tornado after the storm merger. Between 2254–2257 UTC, the Z_{DR} arc extends further back to the mesocyclone, and extends around the tornado at 2259 UTC. Hence, the size-sorting mechanism associated with the low-level mesocyclone is not inhibited significantly by the storm merger. Compared to the merger of Storm C1, the merger of Storm C2 with Supercell B appears to be more disruptive to the storm's dynamics, possibly because Storm C2 was comparatively larger and more intense than Storm C1. However, the storm merger appears to have little impact at low-levels during tornadogenesis, although it is possible the regeneration of the low-level mesocyclone may have proceeded faster in the absence of the storm merger.

4) Impact of second storm merger on tornado intensification

While the Tecumseh tornado is developing, a left-moving supercell is within the inflow region of Supercell B. Hence, the cooled air from the left-moving supercell's FFD might be ingested by the southern storm's updraft and cause it to weaken. Mesonet data from the Bowlegs site is investigated to analyze the thermodynamic characteristics of the FFD downdraft. Unfortunately, the FFD was not located over the Bowlegs site during tornadogenesis (2250 – 2300 UTC), but passed over the Bowlegs site between 2310 and 2315 UTC coincident with a period of tornado intensification. During this period, θ_e values decrease from 71.5 to 70.2°C. Hence, the θ_e deficits within the FFD here are quite small, and thus the buoyancy of air from the FFD remained similar to the environment. Thus, parcels passing through the FFD prior to entering the tornado or mesocyclone remained buoyant.

The storm merger occurs between 2304 and 2330 UTC (from KTLX) after the Tecumseh tornado formed. Intriguingly, the storm merger occurred during the intensification phase of the Tecumseh tornado, indicating that the storm merger did not inhibit tornado intensification, and perhaps enhanced the tornado intensity. As discussed previously, the FFD downdraft exhibited small θ_e deficits, so the left-moving supercell likely did not have a negative impact on the buoyancy of inflow air into the mesocyclone or tornado.

4. CONCLUSIONS

OU-PRIME obtained high-resolution polarimetric radar data on 10 May 2010, capturing the evolution of polarimetric signatures in a tornadic cyclic supercell undergoing several storm mergers and ingesting air from the FFDs of nearby storms.

This paper addresses the need for new studies of cyclic supercells to determine if the cyclic pattern of polarimetric signatures observed by Kumjian et al. (2010) is intrinsic to cyclic supercells. Indeed, this study found that the evolution of the polarimetric signatures generally followed the cyclic pattern they described, and a similar evolution of polarimeric signatures is observed for tornadic and nontornadic cyclic supercells. This result further suggests that the cyclic pattern of polarimetric signatures is linked to the changes in storm dynamics and microphysics throughout the evolution of cyclic supercells. The Z_{DR} arc dissipated during the occlusion of the mesocyclone, and regenerated very quickly during the next cycle (about 5 min). During mesocyclogenesis, Z_{DR} and ρ_{hv} rings reform on the southern flank of the supercell. Moreover, two distinct Z_{DR} rings associated with both the occluded and the new mesocyclone were observed.

The impact of storm mergers on supercells and tornadogenesis is not fully understood (e.g., Wurman et al., 2007), hence this study addresses the need for studies of storm mergers, and develops the application of polarimetric data for assessing the impact of storm mergers on the dynamics and structure of supercells. In this study, the extent of the disruption of the storm's dynamics was dependent upon the depth and intensity of the merging convection. During the merger of more shallow and weaker convection, the maintenance of a Z_{DR} ring suggests that the mid-level mesocyclone maintained intensity during the storm merger. In contrast, during the merger of deeper, more intense convection, the Z_{DR} ring became disorganized. However, the Z_{DR} ring quickly regenerated during the next volume scan, indicating that the mid-level mesocyclone was only disrupted briefly. The Z_{DR} arc actually reforms during the storm merger, indicating that the storm merger process did not inhibit the size sorting mechanism during the storm merger.

A possible application of this study is utilizing polarimetric data to nowcast the evolution of severe storms during storm mergers. Examining the reflectivity field during the storm merger (Figure 11), the storm appears to be rather

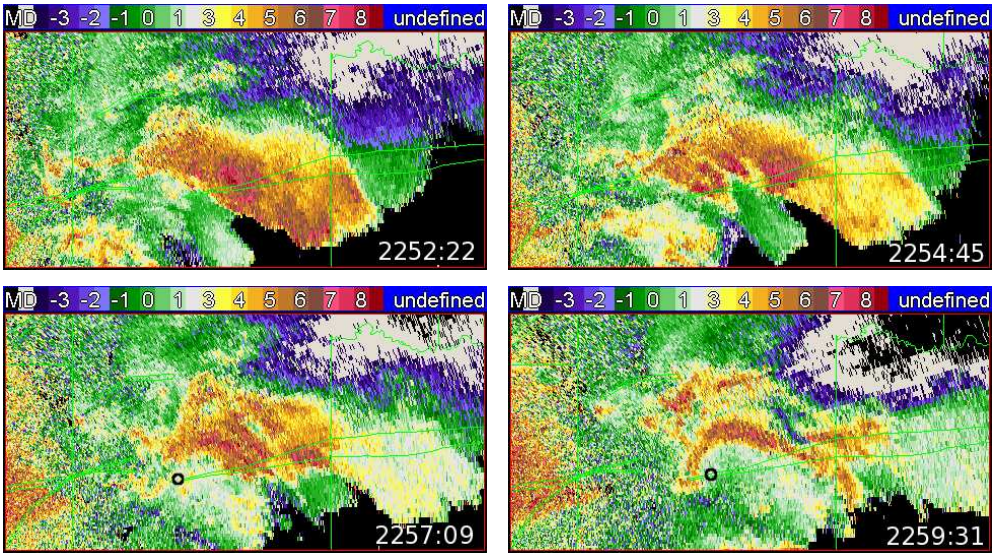

Figure 8: Evolution of the Z_{DR} arc shown in the differential reflectivity Z_{DR} field at the 1°-tilt at 2252, 2254, 2257, and 2259 UTC 10 May 2010. The black circle shows the position of the low-level mesocyclone or tornado, observed in the radial velocity field, on the 2257 and 2259 UTC images.

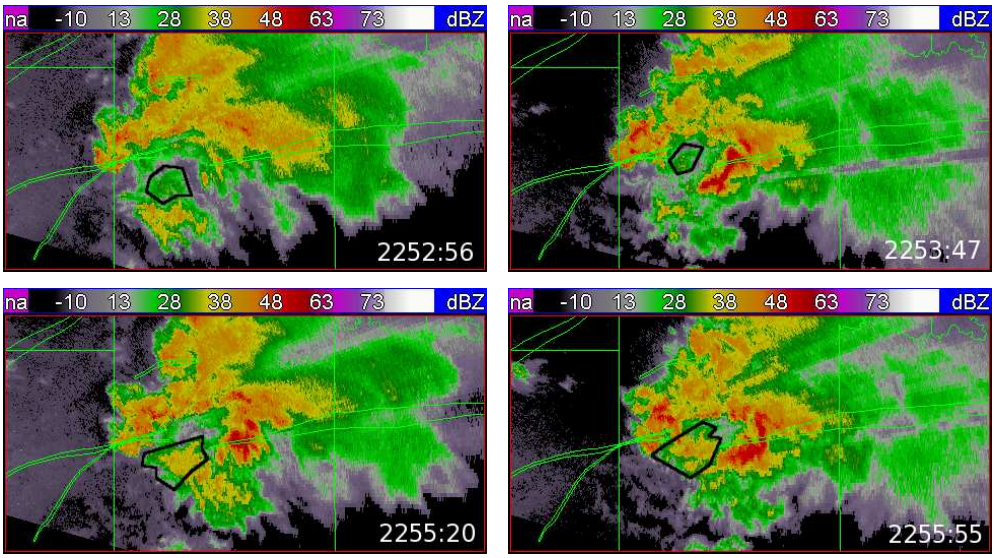

Figure 9: Evolution of low-level reflectivity during mesocyclogenesis and storm mergers at 1°between 2252 – 2259 UTC 10 May 2010.

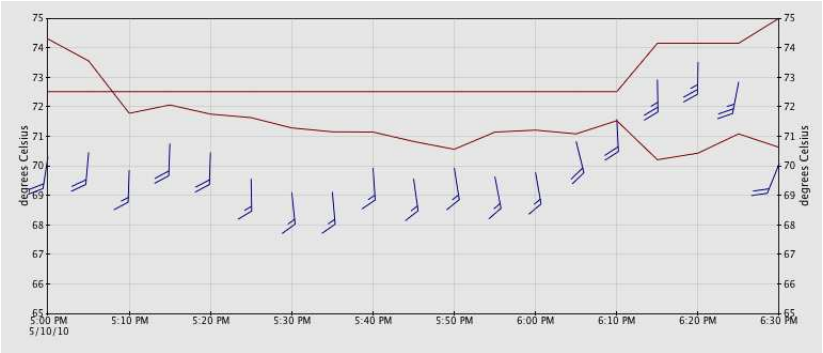

Figure 10: Equivalent potential temperature in °C (θ_e , brown line), rainfall total in mm (blue line), and wind barb from the Bowlegs Mesonet site between 0500 and 0630 PM LT. The half and full wind barbs are 2.5 and 5 m s^{-1}, respectively. As the FFD passes over the SHAW site between 0610 and 0615 PM LT, θ_e decreased from 71.5 to 70.2°C.

disorganized at low-levels and does not suggest imminent tornadogenesis. However, a prominent Z_{DR} arc develops during the storm merger, indicating the increase in size sorting associated with an intensifying low-level mesocyclone. While the Z_{DR} ring became disorganized during the merger for one volume scan, the rapid regeneration of the Z_{DR} ring after the storm merger indicates only a brief disruption of mid-level mesocyclone. Combining the information from these polarimetric signatures, one can infer that the supercell is undergoing mesocyclogenesis and is only temporarily disrupted by the storm merger.

The close proximity of nearby convection produced numerous interactions with the FFDs of nearby convection. In one case, an EF3 tornado formed in the FFD of the supercell to its south. An analysis of Oklahoma Mesonet data revealed that small equivalent potential temperature deficits were observed in two different FFDs, suggesting that the FFD air ingested by the low-level mesocyclones and subsequent tornadoes exhibited similar buoyancy to environmental air. Hence, the impact of ingesting air from nearby storm's FFDs was minimal, at least in terms of buoyancy. The small θ_e deficits in FFDs in tornado cases are consistent with results from Shabbott and Markowski (2006) and Lee et al. (2006).

The evolution of polarimetric signatures in supercells occurred very rapidly, consistent with the findings of Kumjian et al. (2010). In some cases, significant changes in the Z_{DR} arc or Z_{DR} rings occurred in only one volume scan, so the evolution of these polarimetric signatures is difficult to examine without higher temporal resolution. For example, the Z_{DR} ring reformed between the 2254 and 2257 UTC scans, but the Z_{DR} ring could have formed at 2255 UTC and would not have been observed until 2257 UTC owing to limited temporal resolution. Hence, much higher temporal resolution polarimetric radars are needed. To address this need, the Atmospheric Radar Research Center at OU is currently constructing a high temporal resolution, polarimetric phased array radar (Zhang et al., 2008) called the Cylindrical Phased Array Radar.

5. ACKNOWLEDGMENTS

OU-PRIME is maintained and operated by the Atmospheric Radar Research Center (ARRC) of the University of Oklahoma. Oklahoma Mesonet data are provided courtesy of the Oklahoma Mesonet, a cooperative venture between Oklahoma State University and The University of Oklahoma and supported by the taxpayers of Oklahoma. Doug Speheger provided tornado damage paths produced by the Norman, OK NWS WFO. This paper also benefited from discussions with Chris Schwarz and Brad Isom. The authors also thank Boon Leng Cheong, Redmond Kelley, Adam Smith and Pengfei Zhang for their assistance with computing issues, and thank Boon Leng Cheong for operating the radar during the 10 May 2010 outbreak. The first author was also partially supported by an OU Alumni Fellowship.

References

Adlerman, E. J., and K. K. Droegemeier, 2002: The sensitivity of numerically simulated cyclic mesocyclogenesis to variations in physical and computational parameters. *Mon. Wea. Rev.*, **130**, 2671–2691.

Adlerman, E. J., and K. K. Droegemeier, 2005: The dependence of numerically simulated cyclic mesocyclogenesis upon environmental vertical wind shear. *Mon. Wea. Rev.*, **133**, 3595–3623.

Adlerman, E. J., K. K. Droegemeier, and R. Davies-Jones, 1999: A numerical simulation of cyclic mesocyclogenesis. *J. Atmos. Sci.*, **56**, 2045–2069.

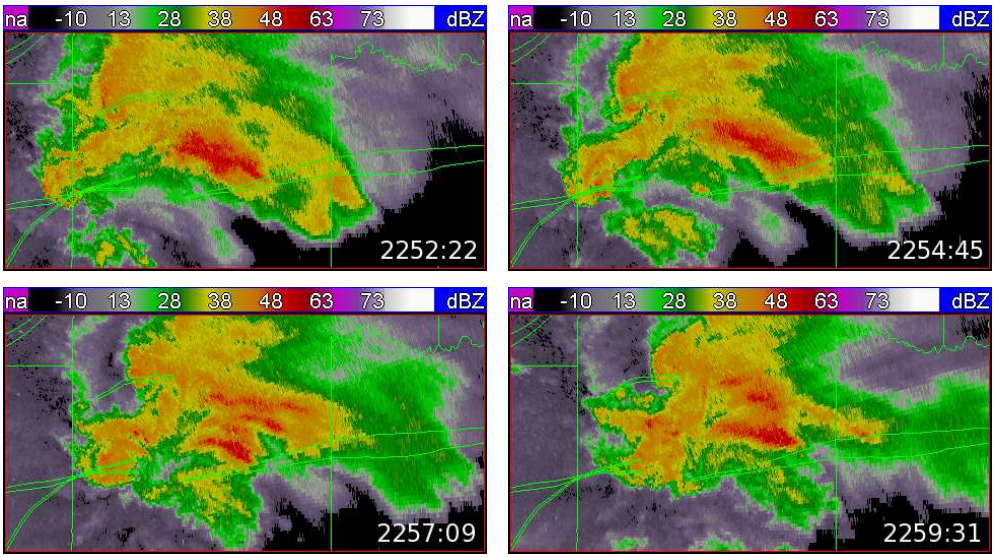

Figure 11: Evolution of low-level reflectivity during mesocyclogenesis and storm mergers at 1°between 2252 – 2259 UTC 10 May 2010.

Beck, J. R., J. L. Schroeder, and J. M. Wurman, 2006: High-resolution dual-Doppler analyses of the 29 may 2001 Kress, Texas cyclic supercell. *Mon. Wea. Rev.*, **134**, 3125–3148.

Bodine, D., R. D. Palmer, C. Ziegler, and P. L. Heinselman, 2010: High-resolution radar analysis during tornadogenesis from OU-PRIME on 10 May 2010. in A. M. Soc., editor, *25th Conf. on Severe Local Storms*, Denver, CO.

Bringi, V. N., V. Chandrasekar, N. Balakrishnan, and D. S. Zrnić, 1990: An examination of radar propagation effects in rainfall at microwave frequencies. *J. Atmos. Oceanic Technol.*, **7**, 829–840.

Brock, F. V., K. C. Crawford, R. L. Elliott, G. W. Cuperus, S. J. Stadler, H. L. Johnson, and M. D. Eilts, 1995: The Oklahoma Mesonet: A technical overview. *J. Atmos. Oceanic Technol.*, **12**, 5–19.

Burgess, D. W., and M. A. Magsig, 1993: Evolution of the Red Rock, Oklahoma supercell of April 26, 1991. in A. M. Soc., editor, *Preprints, 17th Conf. on Severe Local Storms*, St. Louis, MO.

Burgess, D. W., V. T. Wood, and R. A. Brown, 1982: Mesocyclone evolution statistics. in A. M. Soc., editor, *Preprints, 12th Conf. on Severe Local Storms*, pp. 422–424, San Antonio, TX.

Byers, H. R., and R. R. Braham, Jr., 1948: Thunderstorm structure and circulation. *Journal of Meteorology*, **5**, 71–86.

Conway, J. W., and D. S. Zrnić, 1993: A study of production and hail growth using dual-doppler and multiparameter radars. *Mon. Wea. Rev.*, **121**, 2511–2528.

Darkow, G. L., and J. C. Roos, 1970: Multiple tornado producing thunderstorms and their apparent cyclic variations in intensity. in A. M. Soc., editor, *Preprints, 14th Conf. on Radar Meteor.*, pp. 305–308, Tucson, AZ.

Dowell, D. C., and H. B. Bluestein, 2002a: The 8 June 2005 McLean, Texas storm. Part I: Observations of cyclic tornadogenesis. *Mon. Wea. Rev.*, **130**, 2626–2648.

Dowell, D. C., and H. B. Bluestein, 2002b: The 8 June 2005 McLean, Texas storm. Part II: Cyclic tornado formation, maintenance, and dissipation. *Mon. Wea. Rev.*, **130**, 2649–2670.

Fawbush, W. J., and R. C. Miller, 1952: A mean sounding representative of the tornadic air mass environment. *Bull. Amer. Meteor. Sci.*, **33**, 303–307.

French, M. M., H. B. Bluestein, D. C. Dowell, L. J. Wicker, M. R. Kramar, and A. L. Pazmany, 2008: High-resolution, mobile Doppler radar observations of cyclic mesocyclogenesis in a supercell. *Mon. Wea. Rev.*, **136**, 4997–5016.

Fujita, T. T., 1975: New evidence from April 3-4, 1974 Tornadoes. in A. M. Soc., editor, *Preprints, 9th Conf. on Severe Local Storms*, pp. 248–255, Norman, OK.

Hubbert, J., V. N. Bringi, and L. D. Carey, 1998: CSU-CHILL polarimetric measurements from a severe hailstorm in eastern Colorado. *J. Appl. Meteor.*, **37**, 749–755.

Kumjian, M., A. V. Ryzhkov, V. M. Melnikov, and T. J. Schuur, 2010: Rapid-scan super-resolution observations of a cyclic supercell with a dual-polarization WSR-88D. *Mon. Wea. Rev.*, **138**, 3762–3786.

Kumjian, M. R., and A. V. Ryzhkov, 2008: Polarimetric signatures in supercell thunderstorms. *J. Appl. Meteor. Climatol.*, **48**, 1940–1961.

Kumjian, M. R., and A. V. Ryzhkov, 2009: Storm-relative helicity revealed from polarimetric radar measurements. *J. Atmos. Sci.*, **66**, 667–685.

Lakshmanan, V., T. Smith, G. J. Stumpf, and K. Hondl, 2007: The Warning Decision Support System - Integrated Information. *Wea. Forecasting*, **22**, 596–612.

Lee, B. D., B. F. Jewett, and R. B. Wilhelmson, 2006: The 19 April 1996 Illinois tornado outbreak. part II: Cell mergers and associated tornado incidence. *Wea. Forecasting*, **21**, 449–464.

Lei, L., G. Zhang, R. D. Palmer, B. L. Cheong, and M. Xue, 2009: A multi-lag correlation estimator for polarimetric radar variables in the presence of noise. in *34th Conf. on Radar Meteorology*, Williamsburg, VA. Amer. Meteor. Soc.

Lemon, L. R., and C. A. Doswell, 1979: Severe thunderstorm evolution and mesocyclone structure as related to tornadogenesis. *Mon. Wea. Rev.*, **107**, 1184–1197.

Loney, M. L., D. S. Zrnić, J. M. Straka, and A. V. Ryzhkov, 2002: Enhanced polarimetric radar signatures above the melting level in a supercell storm. *J. Appl. Meteor.*, **41**(1179-1194).

Markowski, P. M., E. N. Rasmussen, and J. M. Straka, 1998: The occurence of tornadoes in supercells interacting with boundaries during vortex-95. *Wea. Forecasting*, **13**, 852–859.

Markowski, P. M., J. M. Straka, and E. N. Rasmussen, 2002: Direct surface thermodynamic observations within the rear-flank downdraft of nontornadic and tornadic supercells. *Mon. Wea. Rev.*, **130**, 1692–1721.

McPherson, R. A., C. A. Fiebrich, K. C. Crawford, J. R. Kilby, D. L. Grimsley, J. E. Martinez, J. B. Basara, B. G. Illston, D. A. Morris, K. A. Kloesel, A. D. Melvin, H. Shrivastava, J. M. Wolfinbarger, J. P. Bostic, and D. B. Demko, 2007: Statewide monitoring of the mesoscale environment: A technical update on the Oklahoma Mesonet. *J. Atmos. Oceanic Technol.*, **24**, 301–321.

Oye, R. C., K. Mueller, and S. Smith, 1995: Software for radar translation, editing, and interpolation. in *Preprints, 27th Conf. on Radar Meteorology*, pp. 359–361, Vail, CO. Amer. Meteor. Soc.

Palmer, R. D., D. Bodine, M. Kumjian, B. Cheong, G. Zhang, Q. Cao, H. B. Bluestein, A. Ryzkhov, T.-Y. Yu, and Y. Wang, 2010: The 10 May 2010 tornado oiutbreak in central Oklahoma: Potential for new science with high-resolution polarimetric radar. *Bull. Amer. Meteor. Sci.*, **submitted**.

Palmer, R. D., A. V. Ryzhkov, G. Zhang, B. L. Cheong, T.-Y. Yu, M. B. Yeary, P. B. Chilson, M. I. Biggerstaff, N. L. Hickmon, R. J. Doviak, D. S. Zrnić, M. Knight, N. E. Lawrence, F. Sloan, C. Goode, R. Stafford, R. Keene, P. Neilley, A. Turnbill, J. T. Snow, T. H. L. Williams, and D. Marsh, 2009: OU-PRIME: a high-resolution platform for interdisciplinary polarimetric radar research and education at the University of Oklahoma. in *34th Conf. on Radar Meteorology*, Williamsburg, VA. Amer. Meteor. Soc.

Payne, C. D., T. J. Schuur, D. R. MacGorman, M. I. Biggerstaff, K. M. Kuhlman, and W. D. Rust, 2010: Polarimetric and electrical characteristics of a lightning ring in a supercell storm. *Mon. Wea. Rev.*, **138**, 2405–2425.

Rasmussen, E. N., 2003: Refined supercell and tornado forecast parameters. *Wea. Forecasting*, **18**, 530–535.

Rasmussen, E. N., and D. O. Blanchard, 1998: A baseline climatology of sounding-derived supercells and tornado forecast parameters. *Wea. Forecasting*, **13**, 1148–1164.

Romine, G. S., D. W. Burgess, and R. B. Wilhelmson, 2008: A dual-polarization-radar-based assessment of the 8 May 2003 Oklahoma City tornado supercell. *Mon. Wea. Rev.*, **136**, 2849–2870.

Shabbott, C. J., and P. M. Markowski, 2006: Surface in situ observations within the outflow of forward-flank downdrafts of supercell thunderstorms. *Mon. Wea. Rev.*, **134**, 1422–1441.

Sirmans, D., D. Zrnić, and B. Bumgarner, 1976: Extension of maximum unambiguous Doppler velocity by use of two sampling rates. in A. M. Soc., editor, *Proc. 17th Conf. on Radar Meteorology*, pp. 23–28.

Tabary, P., G. Vulpiani, J. Gourley, A. Illingworth, R. Thompson, and O. Bousquet, 2009: Unusually high differential attenuation at C band: Results from a two-year analysis of the French Trappes polarimetric radar data. *J. Appl. Meteor. Climatol.*, **48**, 2037–2053.

Vulpiani, G., P. Tabary, J. Parent du Chatelet, and F. Marzano, 2008: Comparison of advanced radar polarimetric techniques for operational attenuation correction at C band. *J. Atmos. Oceanic Technol.*, **25**, 1118–1135.

Wurman, J., Y. Richardson, C. Alexander, S. Weygandt, and P.-F. Zhang, 2007: Dual-doppler and single-doppler analysis of a tornadic storm undergoing mergers and repeated tornadogenesis. *Mon. Wea. Rev.*, **135**, 736–758.

Zhang, G., R. Doviak, J. Vivekanandan, W. Brown, and S. A. Cohn, 2004: Performance of correlation estimators for spaced antenna wind measurement in the presence of noise. *Radio Sci.*, **39**, 3017–3033.

Zhang, G., R. Doviak, D. Zrnić, and J. Crain, 2008: Phased array radar polarimetry for weather sensing: challenges and opportunities. in I. International, editor, *Geosci. and Remote Sensing Symp.*, pp. 449–452.